Acta Oceanol. Sin., 2023, Vol. 42, No. 7, P. 175–184
https://doi.org/10.1007/s13131-023-2188-4
http://www.aosocean.com
E-mail: ocean2@hyxb.org.cn

Analysis of wave shoaling and shore-breakers on a low tide terrace beach based on *in-situ* measurements at Xisha Bay on South China coast

Yuan Li[1, 2, 3], Chi Zhang[1, 2*], Hongshuai Qi[4*], Jiacheng Song[5], Weiqi Dai[6], Shanhang Chi[2], Jian Shi[2], Dake Chen[7]

[1] The National Key Laboratory of Water Disaster Prevention, Hohai University, Nanjing 210024, China
[2] College of Harbour, Coastal and Offshore Engineering, Hohai University, Nanjing 210024, China
[3] State Key Laboratory of Estuarine and Coastal Research, East China Normal University, Shanghai 200241, China
[4] Third Institute of Oceanography, Ministry of Natural Resources, Xiamen 361005, China
[5] Shanghai Waterway Engineering Design and Consulting Co., Ltd, Shanghai 200120, China
[6] Yellow River Institute of Hydraulic Research, Yellow River Conservancy Commission, Zhengzhou 450000, China
[7] Nanjing Hydraulic Research Institute, Nanjing 210029, China

Received 7 November 2022; accepted 15 February 2023

Abstract

Low tide terrace beach is a main beach type along South China coasts with strong tidal actions. How strong tides affect wave transformations on low tide terrace beach still remains unclear. In this study, *in-situ* measurements are conducted on the low terrace beach at Xisha Bay to provide quantitative descriptions of wave shoaling and shore-breaker phenomena under the tidal effects. It is found that wave breaking is unsaturated on the low tide terrace beach at Xisha Bay. Magnitudes of wave skewness and asymmetry increase as wave shoals and achieve the maximum value at the shore-breaker, and then decrease rapidly. Mean energy dissipation rates of shore-breakers are tide-modulated since the bottom slope changes at the shoreward boundary of wave propagation in a tidal cycle. The remaining wave energy flux at the initialization of the shore-breaker is 1%–12% of offshore wave energy flux, and the energy flux ratio decreases with increasing offshore wave heights. Wave attenuation at shore-breakers can be estimated directly from offshore wave conditions based on findings in this study, favoring designs of seawalls or beach nourishment projects. Field datasets on wave transformations can also be used for verifications of wave numerical models.

Key words: sandy beach, low tide terrace, waves, shore-breakers, South China coasts

Citation: Li Yuan, Zhang Chi, Qi Hongshuai, Song Jiacheng, Dai Weiqi, Chi Shanhang, Shi Jian, Chen Dake. 2023. Analysis of wave shoaling and shore-breakers on a low tide terrace beach based on *in-situ* measurements at Xisha Bay on South China coast. Acta Oceanologica Sinica, 42(7): 175–184, doi: 10.1007/s13131-023-2188-4

1 Introduction

Sandy coasts provide biological habitats and sites for human recreational activities. Under different driving forces of waves and tides, natural beaches can be classified into various types, i.e., dissipative, intermediate and reflective beach, judged by the dimensionless fall velocity (Wright and Short, 1984). Dissipative beaches are usually found on the high-energy open coastlines. The configuration of dissipation beaches includes a mild sloping intertidal zone and extremely mild subtidal zone (Moulton et al., 2021; Wright et al., 1979). Reflective beaches always develop on low energy headland coastlines, and equips a steep beachface and shoreface. Sandbars are absent on both reflective and dissipative beaches (Chi et al., 2023; Li et al., 2021). Masselink and Short (1993) considered the effect of tidal range on beach states and further dividing the intermediate beach states using the dimensionless relative tidal range. Low tide terrace beach is one typical intermediate beach that often occurs on low-to-medium-energy macrotidal coastlines such as South China coasts (Cai et al., 2022). The configuration of the low tide terrace beach includes a relative steep upper beachface and a low-gradient intertidal zone. A better understanding of tidal effects on hydrodynamic processes on the low tide terrace beach is important for beach nourishments and restorations on South China coasts.

Beach states are highly controlled by surf states, especially on wave-dominated beaches. Although low tide terrace beaches are macrotidal, the role of waves in shaping the morphology cannot be neglected. Surf states on low tide terrace beaches are usually unsaturated. Here, the unsaturated surf means that the increase in offshore wave energy cannot be dissipated totally by wave breaking and thus the inshore wave heights change with offshore

Foundation item: The Key Program of National Natural Science Foundation of China under contract No. 41930538; the Open Research Fund of State Key Laboratory of Estuarine and Coastal Research, East China Normal University under contract No. SKLEC-KF202203; the National Natural Science Foundation of China under contract No. 52201317; the National Key Research and Development Program under contract No. 2022YFC3106102; the China Postdoctoral Science Foundation under contract No. 2022M711023; the Jiangsu Funding Program for Excellent Postdoctoral Talent under contract No. 2022ZB148.
*Corresponding author, E-mail: zhangchi@hhu.edu.cn; qihongshuai@tio.org.cn

wave heights (Baldock et al., 1998). Surf states are judged using the surf similarity parameter proposed by Battjes (1974). Unsaturated surf is usually found on steeper beaches or with low steepness incident waves. The wave breaking zone is narrow or sometimes absent of unsaturated surf and wave breaking can occur near the shoreline very close to or even at the shoreline (Baldock et al., 1998), thus it was defined as "shore-breakers".

The shore-breaker serve as a direct motivation for shoreline changes. It drives swash flows upward, longshore currents downstream and rip currents seaward. Besides, the shore-breaker is also a main factor that threatening the safety of beachgoers. Muller (2018) found the shore-breaker was a contributing factor in over 82% of reported surf-zone injuries in Ocean City, Maryland from 2006 to 2015. However, there is still a scarcity of quantitative research on shore-breakers. For example, how much energy remains at the initialization of shore-breakers? How much is the energy dissipation rate of shore-breakers on the low tide terrace beaches?

The beaches at Xisha Bay on the South China coasts are equipped with a typical "low tide terrace type" morphology, i.e., with a mild dissipative terrace and a steep reflective beachface. Besides, shore-breakers are frequently observed near the shoreline. Therefore, *in-situ* measurements were conducted in this area to provide quantitative description of wave transformations and shore-breakers under the tidal effects.

2 Methods

2.1 *Field measurements and beach states*

Field observations were carried out on the sandy beach of Xisha Bay located on the South China coast. The sandy beach is located on the north side of the Taiwan Strait. The width of the dry beach is approximately 200 m (Fig. 1a). The tidal regime is macrotidal and semi-diurnal with the annually mean tidal range of 4.2 m. Medium-to-coarse sediment with d_{50} = 0.33 mm on the low tide terrace and d_{50} = 0.60 mm on the beachface (Cai et al., 2012). During the beach nourishment project in Xisha Bay, the sediments were filled on the berm to increase the width of the dry beachface. The grain size of filling sediments is approximately two times coarser than native sediments. This is because using coarse sediments can effectively decrease the intensity of sediment motions and to enhance the stability of the upper beachface. As a preliminary estimation, the dimensionless sediment fall velocity and relative tidal range are 1.4 and 10.5, respectively. The dimensionless sediment fall velocity defined as H/w_sT (in which, H and T are the representative wave height and period, and w_s is the sediment settling velocity) describes relative time needed for sediment suspension and settling. The relative tidal range is defined as the magnitude of the breaking wave height and tidal range. The beach state is therefore classified as the low tide terrace according to classic conceptual models of beach types (Wright and Short, 1984; Masselink and Short, 1993). The beach profile in the intertidal zone consists of two parts, i.e., a dissipative low tide terrace with a slope of 1/30 and a reflective high tidal beachface with a slope of 1/10. As can be seen in Fig. 1b, above the high-water level, rhythmic beach cusps can be also found on the beach, corresponding well with the classification of Masselink and Short (1993). As can be seen in Fig. 1c, the x-axis (z-axis) origins at the location (elevation) of dune toe and the positive offshore (upward). The surveyed beach profile ends at the point where the mean low waterline intersects the shoreface. The total length of the survey beach is 142 m.

Field measurements were carried out from 10:00 December 6, 2020 to 10:00 December 8, 2020. Beach profile was measured using the Real-time-kinematic (RTK) at low tides. RTK can obtain real-time positioning data in the field, and the accuracy of the instrument is at the centimeter level, which can greatly improve the efficiency of field work. By comparing the beach profiles measured before and after the two-day field measurements, the morphological changes are found negligible. Time series of wave pressure was recorded using a wave-tidal gauge (RBRsolo^3 D wave16), which is fixed on the bottom and works with sampling frequency of 4 Hz. Six gauges were deployed on the low tide terrace from the seaward boundary to shoreward boundary of the terrace, as can be seen in Fig. 1c.

2.2 *Wave climates*

Offshore wave climates are extracted from a high-resolution wave hindcast database for the Chinese coast. The wave hindcast database (CWAVE) was established using the wave model TOMAWAC forced with the wind field from CFSR database over the whole domain along the coast of the Chinese mainland (Shi et al., 2019). The database can provide wave parameters with high spatial and temporal resolutions. The accuracy of wave hindcasts have been verified using buoy data and satellite altimeter data. The offshore location exhibited in Fig. 1a is chosen by extending the current cross-shore domain to the 20 m water depth. Offshore Root-mean-square (RMS) wave height and mean wave period are provided in Fig. 2, in which t = 0 h corresponds to 10:00 December 6, 2020. It can be found that the offshore wave characteristics are not significantly modulated by tides. Offshore wave heights and periods generally decrease in the first 20 h then increase in the next 20 h, and finally achieve a peak at t = 42 h. Offshore wave heights and periods range from 0.73 m to 1.11 m and from 4.68 s to 7.05 s, respectively. Wave climate in the study area at the time period is modal and storm events are not found.

2.3 *Data processing*

Bottom pressure power density spectrum is computed using the Fast Fourier Transforms, with 10 Hanning windowed, 50% overlapping segments (20 degrees of freedom). The spectrum of bottom pressure is converted into the spectrum of water surface elevation using the classic transferring function method based on the linear wave theory (Bishop and Donelan, 1987). Then, the time series of water surface elevation is obtained using an Inverse Fast Fourier Transform. Raw data was separated into 15 min time series bin to ensure that the still wave level is stationary compared with the changing tidal level, following Power et al. (2010). The bin will be discarded from analysis if the gauge could not be submerged for the full period of 15 min. Wave parameters are calculated after band-pass filter at 0.04 Hz and 1 Hz to remove low frequency motions and instrument noises. The RMS wave height H_{rms} and mean wave period T_{m} are calculated as

$$H_{\mathrm{rms}} = \sqrt{8m_0}, \tag{1}$$

$$T_{\mathrm{m}} = m_0/m_1, \tag{2}$$

where m_0 and m_1 are the 0th and 1st order moment variance of the band-passed filtered water surface. The wave breaking types or surf states can be described using a dimensionless surf similarity parameter ζ_0 (Battjes, 1974),

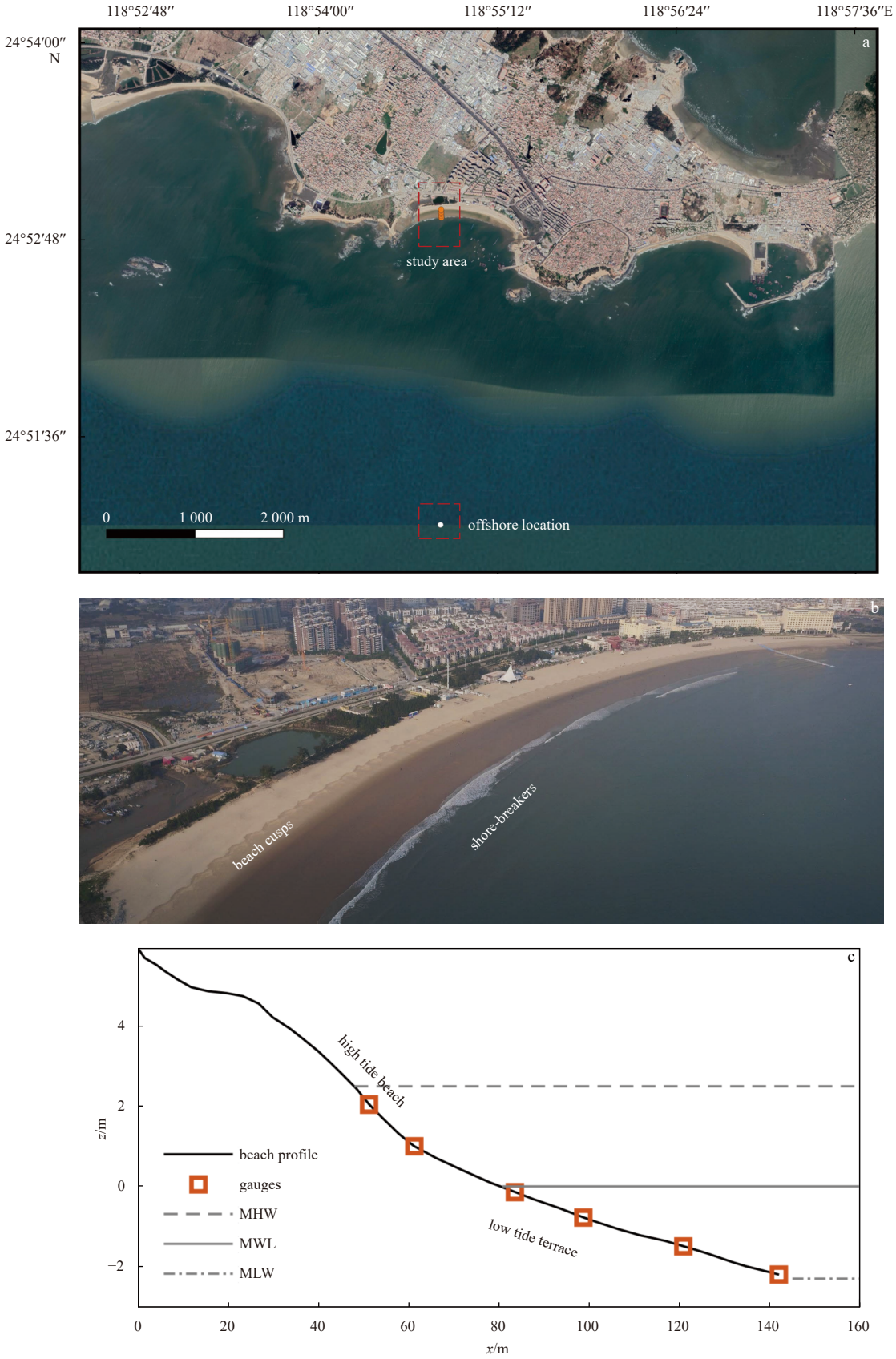

Fig. 1. Map of the study area and the offshore wave location (a); bird's eye view of the study area with shore-breakers and beach cusps (b); beach profile of the study domain and the placements of instruments, tidal levels are obtained by nearby tide station (c). MHW: mean high water level; MWL: mean water level; MLW: mean low water level.

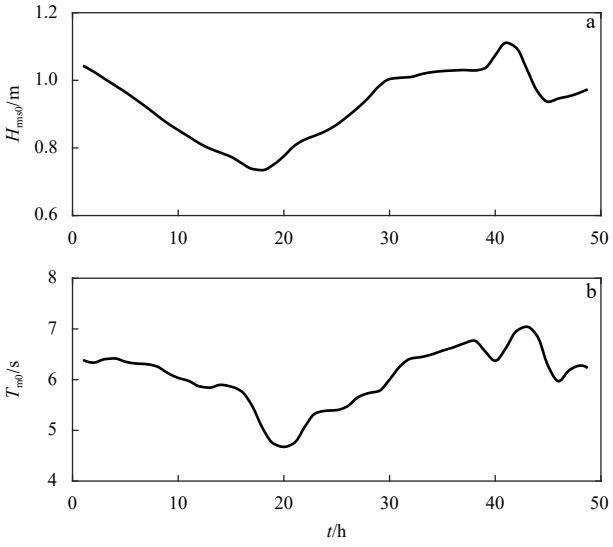

Fig. 2. Time series of offshore RMS wave height (a), and offshore mean wave period (b).

$$\zeta_0 = \frac{m}{\sqrt{H_{\mathrm{rms0}}/L_0}}, \tag{3}$$

where m is the bottom slope of the low tide terrace, H_{rms0} and L_0 are offshore RMS wave height and wave length. ζ_0 of 0.46 is usually used as a threshold for separation of plunging breaker and spilling breaker, as well as the unsaturated surf and saturated surf (Baldock et al., 1998).

Wave shape asymmetry relative to horizontal and vertical axes are described by wave skewness Sk and asymmetry As, which are defined as

$$Sk = \frac{\left\langle (\eta - \overline{\eta})^3 \right\rangle}{\left\langle (\eta - \overline{\eta})^2 \right\rangle^{3/2}}, \tag{4}$$

$$As = \frac{\left\langle \mathbf{H}(\eta - \overline{\eta})^3 \right\rangle}{\left\langle (\eta - \overline{\eta})^2 \right\rangle^{3/2}}, \tag{5}$$

in which, η is water surface elevation, **H** is the Hilbert transformation and the overbar denotes ensemble averaging. Positive Sk means the sharp crests and flat troughs of progressive waves. Similarly, the negative As is characterized by waves with pitch-forward shapes, steep front faces and gentle rear faces (Elgar and Guza, 1985). Ursell number (Ur) is an indicator of normalized integrated bi-amplitude arising from wave nonlinear triad interactions. It has been used as an important dimensionless parameter for parameterizing the Sk and As (Chen et al., 2019; Li et al., 2022a; Peng et al., 2009). The definition of Ur is provided as

$$Ur = \frac{H_{\mathrm{rms}} L_{\mathrm{m}}^2}{d^3}, \tag{6}$$

where the mean wave length calculated with the mean wave period and nonlinear wave celerity in Booij (1981) .

Figure 3 provides the sketch of the shore-breaker near the shoreline. The event of a shore-breaker is identified as the last

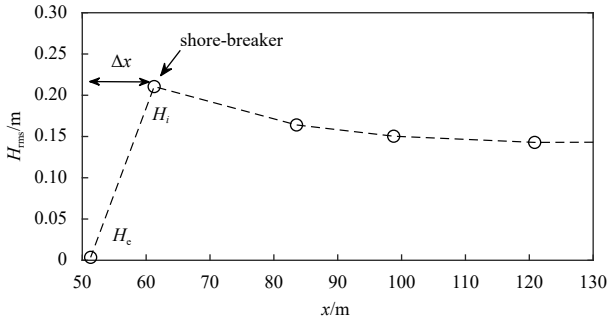

Fig. 3. Sketch of the shore-breaker near the shoreline.

local maximum wave height near the shoreline in Fig. 3, in which the H_e is the representative wave height of the most shoreward gauge, i.e., wave height at the end of the shore-breaker. To ensure the shore-breaker dissipates sufficiently in the distance Δx, measured data with $H_e > 0.05$ m are discarded from the calculation of the energy dissipation of shore-breakers.

The mean energy dissipation D_{bs} of shore-breakers is calculated as

$$D_{\mathrm{bs}} = \frac{Fw_i - Fw_e}{\Delta x}, \tag{7}$$

where $Fw = \frac{1}{8}\rho g H_{\mathrm{rms}}^2 nc$ is the wave energy flux, ρ is the water density, g is the gravity acceleration, n is the ration of wave group velocity to wave phase velocity, c is the wave phase velocity calculated as $c = \sqrt{g(d+0.5H)}$ to take the nonlinear effect into consideration at shallow water depth (Booij, 1981). Note that the wave angles are not considered in Eq. (7) since waves are found to propagate normally respect to the shoreline at shallow water (as can be observed in Fig. 1b). Please refer to Table 1 for a list of the parameters used in this study.

3 Results

3.1 *Wave transformations on the terrace*

As can be seen in Fig. 4a, there are approximately four tidal cycles in the study period. The wave height generally increases to the shoreline (i.e., instantaneous shorelines) and then decreases. Remarkable shore-breakers can be found in front of the shoreline. The wave height of shore-breakers can be up to 0.4 m, which can be almost four times larger than the wave height at the offshore boundary at high tidal levels. At the low tidal levels, wave shoals and breaks in a very short distance on the low tide terrace. At the high tidal levels, a large part of the terrace is dominated by wave shoaling and shore-breakers occur only near the shoreline, as can be seen in Fig. 4b.

To better clarify the wave transformation on the low tide terrace, the cross-shore profiles of RMS wave height and setup at a certain moment $t = 28.75$ h is provided in Fig. 5a. At this moment, wave shoals on the first 60 m of the low tide terrace. The shore-breaker occurs at $x = 82$ m with the maximum wave height of 0.20 m and breaking depth of 1.29 m. The wave setup decreases as wave shoals and achieves a maximum wave set down at the shore-breaker. Shoreward of the shore-breaker, the magnitudes of RMS wave height and wave setup are very small.

The wave height transformation on the low tide terrace beach is different from that on the dissipative beach, on which the wave height decreases from the offshore boundary of the intertidal

Table 1. Notations

Symbol	Definition	Unit
η	wave surface elevation	m
H_{rms}	root-mean-square wave height	m
T_{m}	wave mean period	s
m_n	nth-moment variance of the band-passed filtered water surface elevation	$\mathrm{m^2/s^n}$
H_0	offshore significant wave height	m
Sk	wave skewness	–
As	wave asymmetry	–
Ur	ursell number	–
d	mean water depth	m
ρ	water density	$\mathrm{kg/m^3}$
g	gravity acceleration	$\mathrm{m/s^2}$
c_{g}	wave group velocity	m/s
c	wave celerity	m/s
n	ratio of group velocity to wave celerity	–
D_{bs}	mean energy dissipation rate of shore-breaker	N/ms
F_{w}	wave energy flux	N/s
f_{p}	peak wave frequency	Hz
k	wave number	–

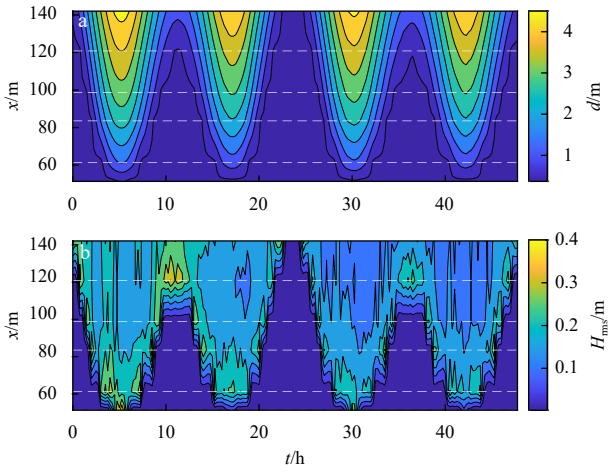

Fig. 4. Spatial and temporal evolution of water depth (a) and RMS wave height (b), the positions of gauges are indicated by white dashed lines.

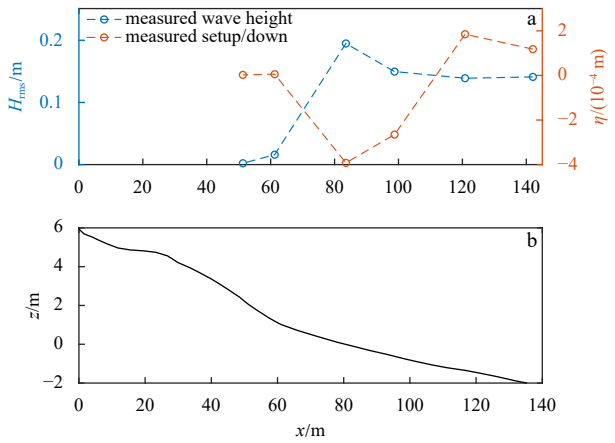

Fig. 5. Cross-shore profile of RMS wave height, wave setup and corresponding beach profile.

zone to the shoreline without obvious wave shoaling processes (Li et al., 2022a). On the low tide terrace, the cross-shore profile of wave height is a typical characteristic of an unsaturated surf with much wave energy remained and finally released near the shoreline, i.e., shore-breakers.

3.2 *Wave nonlinearity evolution*

The time series of *Sk*, *As* and water depth measured with the most offshore gauge are provided in Fig. 6a, since the offshore gauge is submerged most of the time. The magnitudes of *Sk* and *As* are highly modulated by tidal levels, corresponding well with the recent observations on a dissipative beach by Li et al. (2022c). The magnitudes of *Sk* and *As* range from 0.07 to 1.24 and from −1.65 to 0.04, respectively. Their magnitudes generally decrease as water depths increase. Similar observations can also be found on the low-crest breakwater, fringing reef or shoreface nourishment in surf zones (Chen et al., 2019; Li et al., 2022a; Peng et al., 2009). Cross-shore variations of *Sk* and *As* at the certain moment t = 28.75 h (same moment as Fig. 5a) are provided in Fig. 6b. It can be found that *Sk* increases as wave shoals and achieves the maximum value of 0.87 at the shore-breaker, and then decreases rapidly. The magnitude of *As* also increases from 0 to the maximum value of 2.85 at the shore-breaker and then decreases to 0 rapidly. Therefore, the position of the shore-breaker is the critical position where the wave nonlinearity reaches its maximum.

3.3 *Mean energy dissipation rate of shore-breakers*

Time series of mean energy dissipation rate of shore-breakers (D_{bs}) are provided in Fig. 7, with 147 events of shore-breakers identified in total. Note that the event of shore-breaker in this section is identified based on the bulk wave analysis mentioned in Section 2.3 rather than the actual occurrences of shore-breakers in wave-by-wave analysis. D_{bs} generally increases with the offshore water depths, i.e., tidal levels. It can be found that D_{bs} ranges from 0 to 50 N/ms and the surf similarity parameter ζ_0 ranges from 0 to 1.

Positive relations are found between D_{bs} and surf similarity parameter ζ_0. At high tides, D_{bs} is larger than 15 N/ms and ζ_0 is always larger than 0.46. At low tides, D_{bs} is smaller than 15 N/ms and ζ_0 is always smaller than 0.46. This is because that shore-breakers at high tides always occur on the steep beachface, which can promote shore-breakers to occur in the plunging type, as can

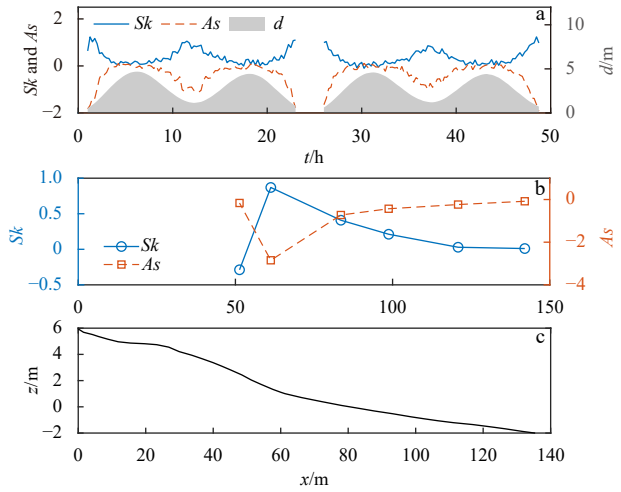

Fig. 6. Time series of nonlinear wave parameters (a); cross-shore profile of *Sk* and *As* (b); corresponding beach profile (c).

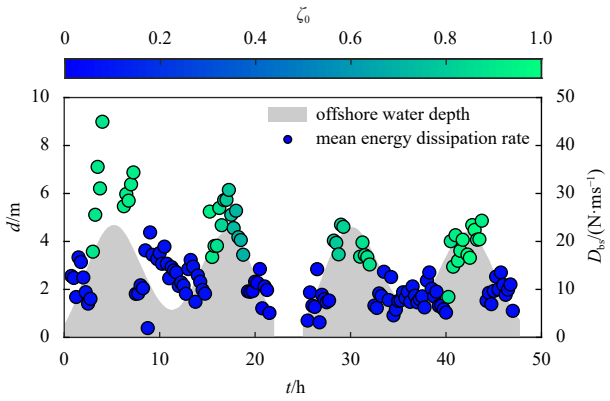

Fig. 7. Time series of mean energy dissipation of shore-breakers.

be seen the snapshot shown in Fig. 8. Breaking waves in the plunging type is more intense and the dissipation of wave energy is more rapid than in the spilling type. While at low tides, shore-breakers usually occur on the relatively mild low tide terrace, which promotes shore-breakers to occur in the spilling type. Therefore, the mean energy dissipation rates of shore-breakers are tide- modulated since the bottom slope changes at the shoreward boundary in tidal cycles. Similar phenomenon such as the tidal modulation of reflected infragravity waves are for the same reason (Thomson et al., 2006; Bertin et al., 2020). This implicates that the wave impact and splashes of plunging breakers can cause beach accidents and the intense shore-breakers at high tides can discourage beachgoers from entering the water, corresponding well with recent findings of Stokes et al. (2017) and de Korte et al. (2021).

4 Discussion

4.1 *Verification of wave nonlinearity formula*

The net near-bed sediment transport rate is well affected by the magnitudes of wave nonlinearities of wave profile, since the near-bed wave orbital velocity is well controlled by the water surface elevation (Rocha et al., 2017; Ruessink et al., 2013). Since estimations of *Sk* and *As* from period-resolving water surface elevations would lead to a huge computational effort when these two parameters are embedded in a beach morphodynamic model, *Sk* and *As* are usually parameterized using *Ur* in the period-averaged framework (Doering and Bowen, 1995; Elfrink et al., 2006; Isobe and Horikawa, 1982; Ruessink et al., 2012). Li et al. (2022c) recently found that the differences between nonlinearities of water surface elevation and wave orbital velocity is not significant when water depths are not very small. In this study, dataset collected on the low tide terrace is also used to verify most recently developed parameterizations of Li et al. (2022a).

Fig. 8. Snapshot of shore-breakers in the plunging type at high tides.

Compared with previous formulas that parameterized on the limited bottom slopes (e.g., on the low-crested breakwater by Peng et al. (2009) and on the fringing reef by Chen et al. (2019)), Li et al. (2022a) proposed new parameterizations of *Sk* and *As* taking both *Ur* and bottom slope into consideration recently. The new parameterizations were found to improve the prediction accuracy especially at shallow water depth in the inner surf zone. These two parameterizations are written as

$$Sk = (-23.08m^2 + 4.99m + 0.1)\ln(Ur) + 95.64m^2 - 20.03m + 0.62, \quad (8)$$

$$As = 1.19\tanh[(92.93m + 12.96)/Ur] - 1.2, \quad (9)$$

where m is the bottom slope of the low tide terrace. The *Sk* and *As* measured in this study are used to evaluate these two new parameterizations. Comparisons of measured and predicted *Sk* and *As* are provided in Fig. 9. Note that the most shoreward gauge is excluded in this comparison, since the magnitudes of measured wave nonlinear parameters are very small and the gauge is above the water most of time. It can be found that new parameterizations of Li et al. (2022a) can provide good predictions when the water depth is large, i.e., at a more offshore position or at high tidal levels. However, the *Sk* is overestimated as the water depth decreases. The phenomenon is obvious when the gauge is placed near the shoreline, where the overestimation is more significant. The predictions of *As* are generally better than *Sk*, though underestimations of the magnitudes of *As* are found at the low tidal levels. The consistent between predicted and measured *As* is good even near the shoreline. This is because Eqs (8) and (9) were also parameterized with intense wave breaking on the shoreface nourishment, where the waves are highly pitched-forward and asymmetric. Thus, the new parameterizations are naturally suitable for predicting *As* of intense shore-breakers.

4.2 *Quantifications of relative wave height*

As mentioned above, the occurrence of shore-breakers indicates the surf processes are unsaturated. Wave height variations in the unsaturated surf can be expressed empirically with the relationship between the relative wave height (H_{rms}/d) and local water depths, beach slopes or offshore wave characteristics (Power et al., 2010; Yao et al., 2020). Based on these empirical relationships, local wave heights can be efficiently calculated when these easy-obtained parameters such as water depths, beach slopes and offshore wave heights are known. In this study, no direct relationship is found between H_{rms}/d and beach slopes (or other combinations of slopes such as m/kd used in Raubenheimer et al. (1996). Therefore, dimensionless parameters combined with local water depth and offshore significant wave height, i.e., kd and d/H_0 are used following Power et al. (2010) and Yao et al. (2019). As can be seen in Fig. 10a, H_{rms}/d generally decreases with kd, and tends to be stable when kd>1. The curve of H_{rms}/d to kd is fitted using the method of nonlinear least squares. The expression of the curve is read as

$$\frac{H_{rms}}{d} = 1.10\ \tanh(-2.69kd) + 1.14, \quad (10)$$

for which, the squared correlation coefficient is 0.54, implying the overall fitness is not very good. Especially when the kd is small and the data points are more scattered. This is in general agree-

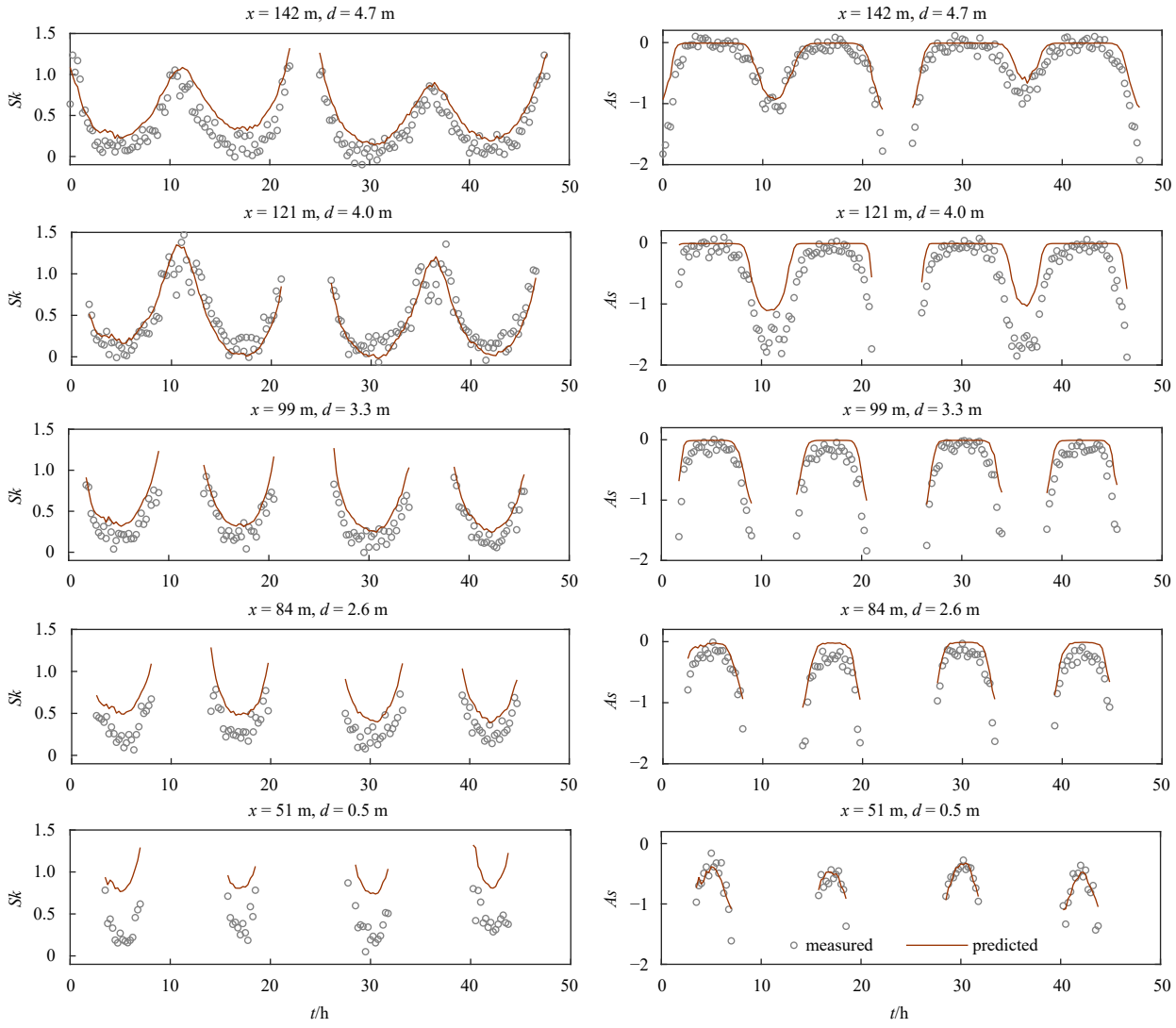

Fig. 9. Comparisons of measured and predicted *Sk* and *As* using new parameterizations of Li et al. (2022a).

ment with previous studies and the same phenomenon can be found in Power et al. (2010), who also conducted observations of wave height variations in the unsaturated surf.

As can be seen in Fig. 10b, H_{rms}/d is found to well relate to d/H_0. H_{rms}/d decreases with increasing of d/H_0 and then tend to be stable. This relationship implies the RMS wave heights in the intertidal zone are affected by offshore wave heights significantly, and they increase with the increasing of the offshore wave heights to a certain level. The phenomenon can provide a direct field evidence for the definition of the unsaturated surf from Baldock et al. (1998). The expression for the fitted curve is written in Eq. (11).

$$\frac{H_{rms}}{d} = -0.78\tanh\left(1.33\frac{d}{H_0}\right) + 0.84. \tag{11}$$

The squared correlation coefficient is 0.85, implying the overall fitness is excellent. However, the fitted curve seems to underestimate the H_{rms}/d at small water depth and tends to a specific upper limit at the shoreline. This is not realistic since the upper limit should not be reached since H_{rms}/d is infinite at the shoreline. Therefore, Eq. (11) is recommended to be used when $d/H_0 > 0.5$ in the unsaturated surfs.

4.3 *Degree of unsaturated surf*

Previous studies provided qualitative descriptions of an unsaturated surf such as the positive relations between inshore wave heights and offshore wave heights, and the occurrence of shore-breakers carrying remaining part of wave energy breaking near the shoreline (Alexander and Holman, 2004; Baldock et al., 1997, 1998; Carini et al., 2021; Power et al., 2010, 2013; Wright et al., 1979). In this section, the ratio of the remaining wave energy flux at the initialization of the shore-breaker to offshore wave energy flux is used as an indicator for quantifying the degree of the unsaturated surf. The remaining wave energy flux at the initialization of the shore-breaker is denoted as Fw_i in Eq. (7) and the offshore wave energy flux is calculated based on the linear wave theory. The remaining wave energy flux at the initialization of the shore-breaker is only a small part of offshore wave energy flux with Fw_i/Fw_0 ranging from 1% to 12%, though in the unsaturated surf. Fw_i/Fw_0 in the first two tidal cycles in the studying period is generally larger than the last two cycles, as can be seen in Fig. 11a. Especially at the high tide of the second tidal cycle, the ratio of energy flux can be up to 12%. Since the offshore wave height achieves its minimum at the second high tide, as can be

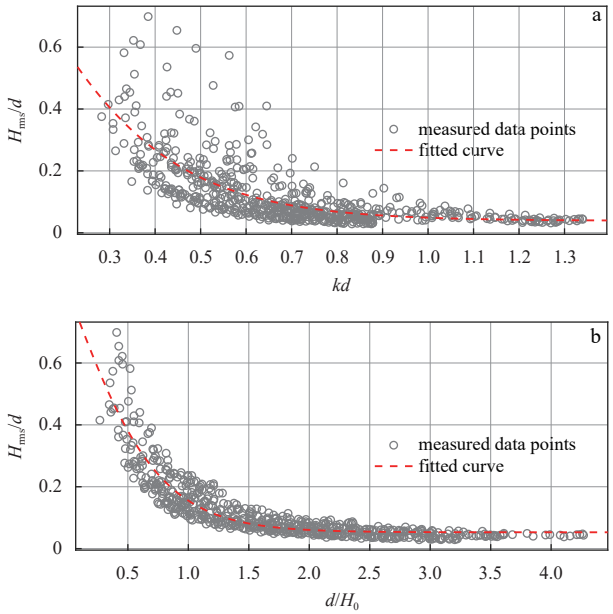

Fig. 10. Relationships between (a) H_{rms}/d and kd; (b) H_{rms}/d and d/H_0.

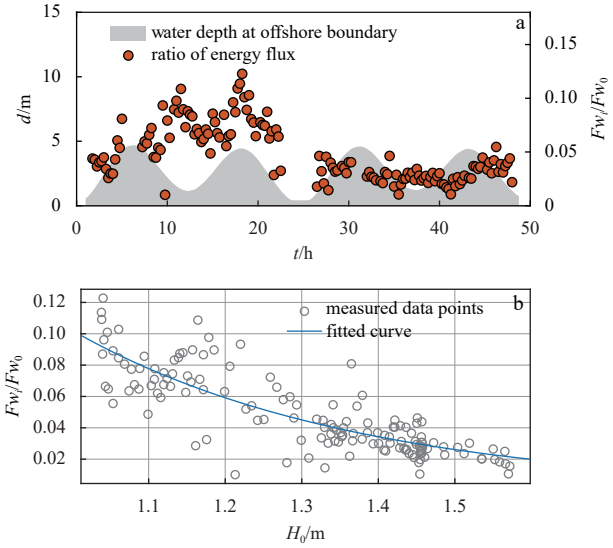

Fig. 11. Time series of Fw_i/Fw_0 and corresponding water levels measured at the offshore boundary of the low tide terrace (a); relationship between Fw_i/Fw_0 and offshore wave height (b).

seen in Fig. 2a, indicating the wave breaking is more unsaturated at this moment. Fw_i/Fw_0 in the last two tidal cycles are more stable and is not modulated by tidal level changes significantly. Hence, Fw_i/Fw_0 is more affected by offshore wave conditions than tidal levels.

A quantitative relationship between Fw_i/Fw_0 and offshore wave heights is illustrated in Fig. 11b. The relationship is read as

$$\frac{Fw_i}{Fw_0} = -0.51\tanh(H_0) + 0.49, \tag{12}$$

for which, the squared correlation coefficient is 0.70, implying the fitness is overall good. Although the dimensions at both ends of the equation are not uniform, this formula focuses on expressing a quantitative relationship rather than detailed physical mechanisms. Fw_i/Fw_0 generally decreases with increasing of offshore wave heights. This is expected since a larger Fw_i/Fw_0 represents a higher degree of the unsaturated surf, which is likely to occur at the milder wave condition (i.e., with smaller offshore wave heights and larger surf similarity parameters). Conversely, a lower degree of the unsaturated surf with a smaller Fw_i/Fw_0 is likely to be found at the storm wave condition with larger offshore wave heights and smaller surf similarity parameters. This can be further explained with the breaking intensification mechanism and breaking resistance mechanism proposed by Zhang et al. (2021a). The breaking intensification mechanism is applied to storm wave conditions. The larger offshore waves evolve to asymmetric shapes and break as water depth decreases on the low tide terrace with the wave breaker index decreases with decreasing of water depth, i.e., waves are easier to break at smaller water depth. In such cases, the remaining wave energy flux near the shoreline is smaller, indicating the degree of the unsaturated surf is lower. The breaking resistance mechanism is applied to mild wave conditions. Under this circumstance, the wave breaker index increases with decreasing of water depth. Smaller waves adapted more sufficiently to the local bathymetry due to shoaling, and they will struggle not to break until a larger breaker index is achieved, i.e., near the shoreline. Thus, the degree of the unsaturated surf is higher.

4.4 *Implications for beach nourishment*

The most important implication of this study relies on its potential guideness on the design of beach nourishment project on low tide terrace beach. The most intense sediment transport and morphological changes occur on the steep beachface at high tides. Shore-breakers in the plunging type release wave energy rapidly thus pick sediments up and mix them in the water column (Ting and Kirby, 1995; Wang et al., 2003; Li et al., 2022b). High concentration of sediments in the water column are either washed upwards by swash flows or carried downstream by alongshore currents, resulting in imbalances of net sediment transport rate and local sediment budget (Chi et al., 2021; Fang et al., 2013; Shi and Kirby, 2008; Zheng et al., 2014; Zhu and Dodd, 2020). Beach nourishments on low tide terrace beaches are mainly conducted by filling sediments on the beachface to enlarge the width of the dry beach (Qi et al., 2010; Shi et al., 2013; Zhao et al., 2021). It is suggested that using coarse sediments is more appropriate for beach nourishments on the low tide terrace beach. On the one hand, the beachface filled with coarse sediments can form a steep slope under the natural adjustments, promoting swash-based wave reflections (Zhang et al., 2021b). On the other hand, relatively low mobility of coarse-grained sediments can enhance the stability of the beachface.

5 Conclusions

Field measurements were conducted on a low tide terrace beach at Xisha Bay on South China coasts. Offshore wave characteristics are obtained by a regional wave hindcast model at water depth of 20 m. Wave pressures were recorded along the low tide terrace and then converted to water surface elevations. RMS wave height, wave skewness and asymmetry are calculated to provide wave shoaling processes. Then, mean energy dissipation rate of shore-breakers as well as the remaining energy flux at the initialization of shore-breakers are analyzed and parameterized. Main conclusions are provided below.

Wave breaking is unsaturated on the low tide terrace beach at the Xisha Bay. The wave height generally increases to the

shoreline and then decreases rapidly. Cross-shore profiles of wave height indicate typical characteristics of shore-breakers that considerable wave energy remained and finally released near the shoreline. Inshore wave heights are found to be well parameterized by local water depths and offshore wave heights.

The magnitudes of wave skewness and asymmetry are highly modulated by tidal levels. Magnitudes of wave skewness and asymmetry increases as wave shoals and achieves the maximum value at the shore-breaker, and then decreases rapidly. Overall trends of the wave skewness and asymmetry are well predicted by recent parameterizations.

Mean energy dissipation rates of shore-breakers are found to be modulated by tidal levels. Mean energy dissipation rates are larger at high tides since waves break on the steep beachface in the plunging type. Conversely, mean energy dissipation rates are small at low tides because waves break on the mild terrace in the spilling type. Besides, the remaining wave energy flux at the initialization of the shore-breaker is only a small part of offshore wave energy flux, ranging from 1% to 12%. The energy flux ratio is found to decrease with the increasing offshore wave heights.

This study highlights the most intense wave breaking and sediment motions modulated by changing tidal levels would occur near the shoreline. Wave attenuation at shore-breakers can be estimated directly from offshore wave conditions based on findings in this study, favoring designs of seawalls or beach nourishment projects. However, only incident short-waves are analyzed in this study. Complete wave energy budget that takes infragravity waves and reflected waves into consideration will be analyzed in future works.

References

Alexander P S, Holman R A. 2004. Quantification of nearshore morphology based on video imaging. Marine Geology, 208(1): 101–111, doi: 10.1016/j.margeo.2004.04.017

Baldock T E, Holmes P, Bunker S, et al. 1998. Cross-shore hydrodynamics within an unsaturated surf zone. Coastal Engineering, 34(3–4): 173–196

Baldock T E, Holmes P, Horn D P. 1997. Low frequency swash motion induced by wave grouping. Coastal Engineering, 32(2–3): 197–222

Battjes J A. 1974. Surf similarity. In: Proceedings of the 14th International Conference on Coastal Engineering. Copenhagen: American Society of Civil Engineers, 466–480

Bertin X, Martins K, de Bakker A, et al. 2020. Energy transfers and reflection of infragravity waves at a dissipative beach under storm waves. Journal of Geophysical Research: Oceans, 125(5): e2019JC015714

Bishop C T, Donelan M A. 1987. Measuring waves with pressure transducers. Coastal Engineering, 11(4): 309–328, doi: 10.1016/0378-3839(87)90031-7

Booij N. 1981. Gravity waves on water with non-uniform depth and current [dissertation]. Delft: Delft University of Technology, 131

Cai Feng, Cao Chao, Qi Hongshuai, et al. 2022. Rapid migration of mainland China's coastal erosion vulnerability due to anthropogenic changes. Journal of Environmental Management, 319: 115632, doi: 10.1016/j.jenvman.2022.115632

Cai Feng, Lei Gang, Chen Xingjun, et al. 2012. Engineering feasibility report on beach restoration project at Xisha Bay, Quanzhou. Xiamen: Third Institute of Oceanography, Ministry of Natural Resources

Carini R J, Chickadel C C, Jessup A T. 2021. Surf zone waves at the onset of breaking: 2. predicting breaking and breaker type. Journal of Geophysical Research: Oceans, 126(4): e2020JC016935

Chen Hongzhou, Jiang Dahuang, Tang Xiaocheng, et al. 2019. Evolution of irregular wave shape over a fringing reef flat. Ocean Engineering, 192: 106544, doi: 10.1016/j.oceaneng.2019.106544

Chi Shanhang, Zhang Chi, Sui Titi, et al. 2021. Field observation of wave overtopping at sea dike using shore-based video images. Journal of Hydrodynamics, 33(4): 657–672, doi: 10.1007/s42241-021-0073-1

Chi Shanhang, Zhang Chi, Wang Ping, et al. 2023. Morphological evolution of paired sand spits at the Fudu River Mouth: wave effects and anthropogenic factors. Marine Geology, 456: 106991, doi: 10.1016/j.margeo.2023.106991

de Korte E, Castelle B, Tellier E. 2021. A Bayesian network approach to modelling rip-current drownings and shore-break wave injuries. Natural Hazards and Earth System Sciences, 21(7): 2075–2091, doi: 10.5194/nhess-21-2075-2021

Doering J C, Bowen A J. 1995. Parametrization of orbital velocity asymmetries of shoaling and breaking waves using bispectral analysis. Coastal Engineering, 26(1–2): 15–33

Elfrink B, Hanes D M, Ruessink B G. 2006. Parameterization and simulation of near bed orbital velocities under irregular waves in shallow water. Coastal Engineering, 53(11): 915–927, doi: 10.1016/j.coastaleng.2006.06.002

Elgar S, Guza R T. 1985. Observations of bispectra of shoaling surface gravity waves. Journal of Fluid Mechanics, 161: 425–448, doi: 10.1017/S0022112085003007

Fang Kezhao, Liu Zhongbo, Zou Zhili, et al. 2013. Numerical simulation of longshore currents. Advances in Water Science (in Chinese), 24(2): 258–265

Isobe M, Horikawa K. 1982. Study on water particle velocities of shoaling and breaking waves. Coastal Engineering in Japan, 25(1): 109–123, doi: 10.1080/05785634.1982.11924340

Li Yuan, Zhang Chi, Chen Dake, et al. 2021. Barred beach profile equilibrium investigated with a process-based numerical model. Continental Shelf Research, 222: 104432, doi: 10.1016/j.csr.2021.104432

Li Yuan, Zhang Chi, Chen Shubin, et al. 2022a. Influence of artificial sandbar on nonlinear wave transformation: experimental investigation and parameterizations. Ocean Engineering, 257: 111540, doi: 10.1016/j.oceaneng.2022.111540

Li Yuan, Zhang Chi, Dai Weiqi, et al. 2022b. Laboratory investigation on morphology response of submerged artificial sandbar and its impact on beach evolution under storm wave condition. Marine Geology, 443: 106668, doi: 10.1016/j.margeo.2021.106668

Li Yuan, Zhang Chi, Song Jiacheng, et al. 2022c. Tide-modulated wave characteristics and breaking regimes in the intertidal zone of a dissipative beach. Ocean Engineering, 266: 113055, doi: 10.1016/j.oceaneng.2022.113055

Masselink G, Short A D. 1993. The effect of tide range on beach morphodynamics and morphology: a conceptual beach model. Journal of Coastal Research, 9(3): 785–800

Moulton A M B, Hesp P A, da Silva G M, et al. 2021. Surfzone-beach-dune interactions along a variable low wave energy dissipative beach. Marine Geology, 435: 106438, doi: 10.1016/j.margeo.2021.106438

Muller M W. 2018. Beach replenishment and surf-zone injuries along the coast of Delmarva, USA. Ocean & Coastal Management, 151: 127–133

Peng Zhong, Zou Qingping, Reeve D, et al. 2009. Parameterisation and transformation of wave asymmetries over a low-crested breakwater. Coastal Engineering, 56(11–12): 1123–1132

Power H E, Baldock T E, Callaghan D P, et al. 2013. Surf zone states and energy dissipation regimes — A similarity model. Coastal Engineering Journal, 55(1): 1350003-1–1350003-18

Power H E, Hughes M G, Aagaard T, et al. 2010. Nearshore wave height variation in unsaturated surf. Journal of Geophysical Research: Oceans, 115(C8): C08030

Qi Hongshuai, Cai Feng, Lei Gang, et al. 2010. The response of three main beach types to tropical storms in South China. Marine Geology, 275(1–4): 244–254

Raubenheimer B, Guza R T, Elgar S. 1996. Wave transformation across the inner surf zone. Journal of Geophysical Research: Oceans, 101(C11): 25589–25597, doi: 10.1029/96JC02433

Rocha M V L, Michallet H, Silva P A. 2017. Improving the parameterization of wave nonlinearities—The importance of wave steep-

ness, spectral bandwidth and beach slope. Coastal Engineering, 121: 77–89, doi: 10.1016/j.coastaleng.2016.11.012

Ruessink G B, Michallet H, Bonneton P, et al. 2013. GLOBEX: wave dynamics on a gently sloping laboraty beach. In: Proceedings of 7th International Conference on Coastal Dynamics. Arcachon: University of Bordeaux, 1351–1362

Ruessink B G, Ramaekers G, van Rijn L C. 2012. On the parameterization of the free-stream non-linear wave orbital motion in nearshore morphodynamic models. Coastal Engineering, 65: 56–63, doi: 10.1016/j.coastaleng.2012.03.006

Shi Fengyan, Cai Feng, Kirby J T, et al. 2013. Morphological modeling of a nourished bayside beach with a low tide terrace. Coastal Engineering, 78: 23–34, doi: 10.1016/j.coastaleng.2013.03.005

Shi Fengyan, Kirby J T. 2008. Discussion of "Wave setup and setdown generated by obliquely incident waves" by T.-W. Hsu et al., coastal engineering, 53, 865-877, 2006. Coastal Engineering, 55(12): 1247–1249, doi: 10.1016/j.coastaleng.2008.08.001

Shi Jian, Zheng Jinhai, Zhang Chi, et al. 2019. A 39-year high resolution wave hindcast for the Chinese coast: model validation and wave climate analysis. Ocean Engineering, 183: 224–235, doi: 10.1016/j.oceaneng.2019.04.084

Stokes C, Masselink G, Revie M, et al. 2017. Application of multiple linear regression and Bayesian belief network approaches to model life risk to beach users in the UK. Ocean & Coastal Management, 139: 12–23

Thomson J, Elgar S, Raubenheimer B, et al. 2006. Tidal modulation of infragravity waves via nonlinear energy losses in the surfzone. Geophysical Research Letters, 33(5): L05601

Ting F C K, Kirby J T. 1995. Dynamics of surf-zone turbulence in a strong plunging breaker. Coastal Engineering, 24(3–4): 177–204

Wang Ping, Ebersole B A, Smith E R. 2003. Beach-profile evolution under spilling and plunging breakers. Journal of Waterway, Port, Coastal, and Ocean Engineering, 129(1): 41–46

Wright L D, Chappell J, Thom B G, et al. 1979. Morphodynamics of reflective and dissipative beach and inshore systems: southeastern Australia. Marine Geology, 32(1–2): 105–140

Wright L D, Short A D. 1984. Morphodynamic variability of surf zones and beaches: a synthesis. Marine Geology, 56(1–4): 93–118

Yao Yu, He Wenrun, Deng Zhengzhi, et al. 2019. Laboratory investigation of the breaking wave characteristics over a barrier reef under the effect of current. Coastal Engineering Journal, 61(2): 210–223, doi: 10.1080/21664250.2019.1579461

Yao Yu, He Wenrun, Jiang Changbo, et al. 2020. Wave-induced set-up over barrier reefs under the effect of tidal current. Journal of Hydraulic Research, 58(3): 447–459, doi: 10.1080/00221686.2019.1623928

Zhang Chi, Li Yuan, Cai Yu, et al. 2021a. Parameterization of nearshore wave breaker index. Coastal Engineering, 168: 103914, doi: 10.1016/j.coastaleng.2021.103914

Zhang Chi, Li Yuan, Zheng Jinhai, et al. 2021b. Parametric modelling of nearshore wave reflection. Coastal Engineering, 169: 103978

Zhao Shaohua, Cai Feng, Liu Zhifei, et al. 2021. Disturbed climate changes preserved in terrigenous sediments associated with anthropogenic activities during the last century in the Taiwan Strait, East Asia. Marine Geology, 437: 106499, doi: 10.1016/j.margeo.2021.106499

Zheng Jinhai, Zhang Chi, Demirbilek Z, et al. 2014. Numerical study of sandbar migration under wave-undertow interaction. Journal of Waterway, Port, Coastal, and Ocean Engineering, 140(2): 146–159

Zhu Fangfang, Dodd N. 2020. Swash zone morphodynamic modelling including sediment entrained by bore-generated turbulence. Advances in Water Resources, 146: 103756, doi: 10.1016/j.advwatres.2020.103756